J Mater Sci (2007) 42:7806–7811
DOI 10.1007/s10853-007-1626-6

Structural unit and faceting description of Σ3 asymmetric tilt grain boundaries

Mark A. Tschopp · David L. McDowell

Received: 7 November 2006 / Accepted: 16 February 2007 / Published online: 24 May 2007

Abstract Atomistic simulations are employed to investigate the structure of Σ3 asymmetric tilt grain boundaries (ATGBs) with boundary planes rotated about the ⟨110⟩ misorientation axis in Cu and Al. Results show that the structural units (SUs) and faceting of all 25 Σ3 ATGBs in Cu and Al intermediate to the coherent twin boundary and the symmetric incoherent twin boundary can be completely defined in terms of SUs for these two symmetric boundaries. A structural unit and faceting description for Σ3 asymmetric tilt grain boundaries is presented. Interestingly, this description is identical for both low stacking fault energy Cu and high stacking fault energy Al; only the dissociation width of the D structural unit on the incoherent twin facet differs in Cu and Al. A model based upon the coincidence plot and the structural units of the Σ3 coherent and incoherent twin boundaries is shown to accurately describe the structural units and faceting for all calculated Σ3 asymmetric tilt grain boundaries in this study. This model can also be extended to continuum descriptions of these boundaries to facilitate higher scale computational models.

Grain boundaries (GBs) significantly impact the bulk properties of polycrystalline materials [1]. However, GBs have a range of functional or mechanical properties. Certain low order coincident site lattice (CSL) boundaries such as Σ3 GBs have properties that differ from other general GBs. The difference in properties is indicative of the underlying difference in GB structures at the nanoscale. The GB structure changes as a function of the misorientation angle between the two adjacent crystal lattices (e.g., [2, 3]). This concept dates back to the work of Bishop and Chalmers [4] on the coincidence of GB ledges in boundaries. Many atomistic studies on GB structure focus on symmetric tilt grain boundaries (STGBs) and show that each GB can be divided into individual structural units (SUs). Each SU corresponds to a particular favored GB misorientation angle and GBs with intermediate misorientation angles are composed of a combination of SUs from these favored GBs. The structural unit model was formulated to predict the structure of STGBs in Cu and Al by Sutton and Vitek [2]. Later, with different potentials, Rittner and Seidman [3] examined the SUs of STGBs with a ⟨110⟩ misorientation axis for both low and high stacking fault energy materials. They show that while the structural unit model holds for many GBs, it is not universally valid; the SU description of many GBs in low stacking fault energy materials cannot be predicted from this model. Additionally, asymmetry due to inclination of the GB plane from the symmetric orientation is described through microfaceting [5]. However, the link between faceting and structural units may be difficult to establish for many asymmetric tilt grain boundaries (ATGBs) due to local atomic rearrangements that minimize the total energy of the boundary.

While most atomistic studies of GB structure focus on STGBs, very few studies in comparison focus on the structure of ATGBs. Simulations of STGBs have focused on an improved understanding of the grain boundary structural makeup [2, 6–8] as well as interface structure-property relationships, such as the influence of structure on GB diffusion [9, 10], GB migration [11, 12], or GB

M. A. Tschopp
School of Materials Science and Engineering, Georgia Institute of Technology, 801 Ferst Drive, Atlanta, GA 30332-0245, USA

D. L. McDowell (✉)
G.W. Woodruff School of Mechanical Engineering,
School of Materials Science and Engineering, Georgia Institute of Technology, 801 Ferst Drive, Atlanta, GA 30332-0245, USA
e-mail: david.mcdowell@me.gatech.edu

mechanical behavior [13–17]. In general, these studies show that the interface structure at the nanoscale plays an important role in determining interfacial properties. Conversely, simulations of ATGBs have mainly focused on specific grain boundary planes to help explain the observed GB structure (e.g., the 9R phase) from HRTEM images [cf. 18–21] or calculate certain GB properties (e.g., the shear deformation response of a few specific ATGBs [14] or the GB mobility and self-diffusivity properties of Σ5 ATGBs [22]). Perhaps the most extensive work on Σ3 ATGB structure at an atomic level combines experimental HRTEM images with calculated atomistic structures for the Σ3 ATGB system in Cu [23, 24]; in contrast to this study, the current study examines the effect of stacking fault energy in face-centered cubic (FCC) metals (both Cu and Al) and characterizes the atomic ATGB structures in terms of structural units and facets with a methodology motivated by the structural unit model of Sutton and Vitek [2].

Many experimental studies at the macroscale, on the order of microns, investigate the Σ3 system in relation to the grain boundary character distribution in polycrystals [26–29] and the faceting and de-faceting of ATGBs as a function of temperature, impurity content, or material system [30–36]. Other experimental studies show that the grain boundary plane in Σ3 boundaries influences macroscale properties, such as GB energy [23, 24], GB diffusion [37], or intragranular corrosion resistance [38]. An improved understanding of the structure and faceting of Σ3 ATGBs through atomistic simulations can complement existing experimental work on this low-order coincident site lattice system.

In this work, the structure of Σ3 ATGBs is investigated as a function of inclination angle about the ⟨110⟩ tilt axis for Cu and Al; a structural unit and faceting description is found for the aforementioned class of ATGBs. First, molecular statics simulations show that all Σ3 ATGBs can be decomposed into atomistic facets that correspond to the two Σ3 STGBs (i.e., the coherent twin boundary (CTB) and the symmetric incoherent twin boundary (SITB)). On each of these facets, the only SUs present are those belonging to the CTB and SITB. Then, these ATGB structures are used to formulate a model that can predict both the SU and faceting description for all Σ3 ATGBs using only the coincident plot and the SUs of the coherent and incoherent twin (symmetric tilt) boundaries. The ability to predict the faceted behavior and SU description for Σ3 ATGBs not only provides a better understanding of the structure of ATGBs, but can also be extended to other models that can incorporate GB structure, such as dislocation dynamics or phase field models. Additionally, the applicability of a model that predicts the structural unit and faceting description of Σ3 ATGBs may help to determine both the individual properties of Σ3 ATGBs and the bulk properties of polycrystals.

Table 1 lists the 25 Σ3 GBs investigated in this research, which consist of 23 ATGBs and 2 STGBs (i.e., the CTB and SITB). In the CSL notation, the designation Σ3 denotes that if the two adjoining crystal lattices are allowed to overlap, one in every three points is coincident. This occurs for a specific misorientation angle $\theta = 70.53°$ and all 25 grain boundaries in this study are misoriented by 70.53°. However, the misorientation angle θ merely expresses the rotation between the two lattices and does not consider the two additional degrees of freedom relating to the GB plane. For this purpose, the term inclination angle Φ is used to define the relative rotation of the GB plane about the tilt axis. We define the CTB as $\Phi = 0°$ and the SITB as $\Phi = 90°$. All other intermediate inclination angles are Σ3 ATGBs. Another method of characterizing the GB plane is to define the GB normals of the two adjoining lattices (e.g., $(hkl)_1/(hkl)_2$). In this work, Σ3 ATGBs are defined using both notations (e.g., $\Sigma 3(554)_1/(11\bar{8})_2\Phi = 64.76°$). Note that the twist angle for all boundaries is 0°.

A computational cell with Born-von Karman (3D) periodic boundary conditions consisting of two grains is used to obtain the equilibrium 0 K structure for each ATGB (cf. [3]). The minimum distance between the two periodic boundaries in each computational cell is at least 5 nm. Over 2700 initial configurations with different in-plane rigid body translations and an atom deletion criterion are used to access the minimum energy GB structures; some ATGBs have accessibilities [3] as low as 0.1%. A nonlinear conjugate gradient algorithm is used for energy minimization. We use Cu and Al embedded-atom method potentials [39, 40] that reproduce stacking fault energies (stable and unstable) consistent with available experimental data and *ab initio* calculations. Additionally, this methodology yields GB energies that are in agreement with both calculated and experimentally measured energies for Σ3 ATGBs [23, 24] as given in Ref. 25. Furthermore, the GB structures associated with these energies are also in agreement with several experimentally observed HRTEM structures for Σ3 ATGB structures with the 9*R* structure (e.g., in Cu [24] and Ag [18, 20]).

Figure 1 shows six of the Cu GB structures obtained using the aforementioned methodology. The SUs for these structures are identified by using a threshold value (0.25) for the centrosymmetry parameter [41] as a guideline to delineate atoms belonging to SUs from those of the bulk lattice. The structures are viewed along the $[1\bar{1}0]$ tilt axis and the atoms on two consecutive $(2\bar{2}0)$ planes are shown as black and white. The GB normal and period vectors for the lower and upper crystal are shown in the corner boxes on the left-hand for each GB. The two arrows in the upper right corner correspond to the ideal location of the CTB

Table 1 The inclination angles and GB normals for the 25 GBs investigated in this study

Inclination Angle Φ	GB Planes $(hkl)_1/(hkl)_2$	Inclination Angle Φ	GB Planes $(hkl)_1/(hkl)_2$
0.00°	$(11\bar{1})_1/(111)_2$	48.53°	$(331)_1/(1,1,13)_2$
6.21°	$(14,14,\bar{1}1)_1/(445)_2$	54.74°	$(221)_1/(001)_2$
10.02°	$(33\bar{2})_1/(7,7,10)_2$	60.50°	$(332)_1/(1,1,\bar{1}4)_2$
13.26°	$(77\bar{4})_1/(558)_2$	62.06°	$(775)_1/(1,1,\bar{1}1)_2$
15.79°	$(22\bar{1})_1/(447)_2$	64.76°	$(554)_1/(1,1,\bar{8})_2$
19.47°	$(55\bar{2})_1/(112)_2$	67.01°	$(887)_1/(2,2,\bar{1}3)_2$
22.00°	$(33\bar{1})_1/(5,5,11)_2$	70.53°	$(111)_1/(11\bar{5})_2$
25.24°	$(44\bar{1})_1/(225)_2$	74.21°	$(778)_1/(11\bar{4})_2$
29.50°	$(77\bar{1})_1/(113)_2$	76.74°	$(445)_1/(22\bar{7})_2$
35.26°	$(110)_1/(114)_2$	79.98°	$(557)_1/(11\bar{3})_2$
40.32°	$(881)_1/(2,2,11)_2$	81.95°	$(223)_1/(4,4,\bar{1}1)_2$
43.31°	$(551)_1/(117)_2$	90.00°	$(112)_1/(11\bar{2})_2$
46.69°	$(772)_1/(1,1,10)_2$		

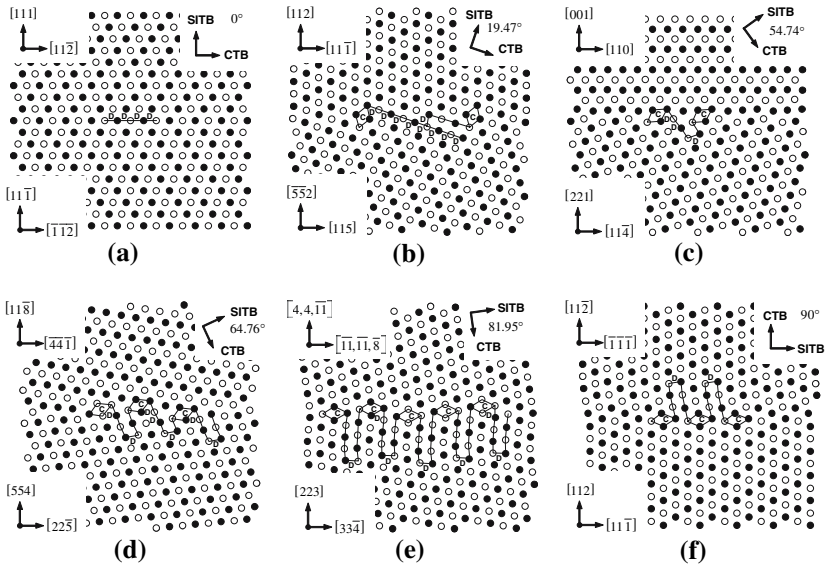

Fig. 1 Six Σ3 GB structures in Cu for various inclination angles. The structures are viewed along the $[1\bar{1}0]$ tilt axis; atoms on consecutive $(2\bar{2}0)$ planes are shown as black and white. The GB normal and period vectors for the lower and upper crystal are shown in the left-hand corner boxes while the inclination angle and facet alignments are shown in the upper right-hand corner

and SITB facets based on the inclination angle (also shown).

The CTB and the SITB (i.e., the two Σ3 STGBs) are shown in Fig. 1a and 1f, respectively. The same notation as in Ref. 3 is used to identify structural units; the CTB period has two D SUs while the SITB period has a dissociated D SU and a C SU. First, notice that the four Σ3 ATGBs in Figs. 1b–1e are described using only the SUs of the two Σ3 STGBs. All Σ3 ATGBs inclined about the ⟨110⟩ tilt axis in both Al and Cu are composed of these same Σ3 STGB SUs. Once all boundaries are described in terms of the C and D SUs, these SUs can be associated with either the CTB or SITB facets (e.g., compare the SUs with the upper left-hand arrows). Following the structure of the Σ3 STGBs, the D SUs correspond to CTB facet while the |*DC*| SUs are on the SITB facet. This atomic level faceting is more obvious for lower inclination angles for which the D SUs associated with the CTB facet significantly outnumber the |*DC*| SUs of the SITB facet (see Fig. 1b). This faceting is less obvious for higher inclination angles (Fig. 1c–1e) due to the large number of atoms affected by the dissociated D SU of the SITB facet, but it is observed nonetheless. Also, notice that the $\Sigma 3(223)_1/(4,4,\bar{1}1)_2\Phi = 81.95°$ GB in Fig. 1e contains the 9*R* phase for Cu. The 9*R* phase is not present in Al, though. The 9*R* phase stacking sequence is formed by an intrinsic stacking fault on every third plane that is caused by the dissociation of the D SUs on the SITB facets. The model for structural unit and faceting described in this work predicts the atomistic SU description for Cu (Al), regardless of the presence (absence) of the 9*R* phase.

The structural unit and faceting description for these six GBs is given in Table 2. This SU notation is slightly

Table 2 Structural unit and faceting description for the 6 grain boundaries in Fig. 1

Inclination Angle Φ	GB Normals $(hkl)_1/(hkl)_2$	Grain Boundary Structural Unit Description	SITB facet # of |*DC*| SUs	CTB facet # of D SUs
0.00°	$(11\bar{1})_1/(111)_2$	|*D.D*|	0	2
19.47°	$(55\bar{2})_1/(112)_2$	|4(*D.D*)/*DC*|	1	8
54.74°	$(221)_1/(001)_2$	|*D.D*/*DC*|	1	2
64.76°	$(554)_1/(11\bar{8})_2$	|*D.D*/*DC*/*D*/*.D.C*/*.D*/*DC*|	3	4
81.95°	$(223)_1/(4,4,\bar{1}1)_2$	|*D*/*.D.C.D.C.D.C*/*.D*/*DCDC*|	5	2
90.00°	$(112)_1/(11\bar{2})_2$	|*DC*|	1	0

modified from that used for STGBs (e.g., [2]) as well as in previous works on ATGBs [5]. For instance, this SU description for Σ3 ATGBs identifies the SUs, the GB period, the relative displacement of SUs in the tilt axis direction, *and* the facet that the SU belongs to. The vertical bars around the structure denote one GB period perpendicular to the tilt axis, while the dot preceding an individual SU signifies a relative translation of $a_0/4[110]$ along the tilt axis from other similar SUs. The slash is used to represent a transition from one facet to another; all GB structures start on the CTB facet. This notation helps to distinguish D SUs on the CTB facet from D SUs on the SITB. Last, the notation 4(D.D) denotes that there are 8 D SUs on this CTB facet that alternate with respect to their relative translation in the tilt axis direction. The ratio of D SUs on the CTB facets to the |*DC*| units on the SITB facets decreases as the inclination angle increases. The model for the structural unit and faceting description in this work predicts the correct ratios as well as the correct number of SUs on each facet when compared to the 23 calculated ATGB structures.

The Σ3 ATGB structures for Cu and Al are also compared to investigate the differences in GB structure between a low (Cu) and high (Al) stacking fault energy material. The GB structures only differ with respect to the dissociation width. The D SU on the SITB facet does not dissociate as far in Al as in the Cu Σ3 ATGBs. Therefore, the 9R phase is not observed in Al. However, the GB structures are otherwise identical between the two FCC materials in terms of structural units and faceting. The GB structures listed in Table 2 are also applicable for Al; i.e., the $\Sigma 3(554)_1/(11\bar{8})_2\Phi = 64.76°$ ATGB has a |*D.D*/*DC*/*D*/*.D.C*/*.D*/*DC*| structure in both Al and Cu. This relationship holds for all Σ3 ATGB structures. This implies that a model that predicts the structural unit and faceting description of Σ3 ATGBs may be applicable to both low and high stacking fault energy FCC metals, even though the D SU on the SITB facet will dissociate more in low stacking fault energy FCC materials.

In a method similar to the structural unit model, the atomic SUs and their corresponding facets can be predicted for Σ3 ATGBs. Figure 2 shows how the calculated Σ3 ATGB structures for Cu and Al can be predicted based upon the coincidence plot [42] and the atomistic GB structures of the two Σ3 STGBs. In this respect, the following method used for predicting the Σ3 ATGB structure is very similar to the decomposition lattice method (cf. [2]) or strip method of quasicrystallography (cf. [1, 43]); the strip method is used to determine the structural unit sequence for rational symmetric tilt boundaries. First, as shown in Fig. 2a, the coincidence plot is created by defining a misorientation angle (i.e., $\theta = 70.53°$ in this case) and allowing the two crystal lattices to overlap. In this plot, atoms from the two lattices are shown as small black and large white circles; the coincident sites are a combination of both circles. The coincidence plot visually illustrates the CSL concept for symmetric and asymmetric tilt grain boundaries; notice that one in every three points is coincident, as denoted by the solid lines in (a).

The GB plane is then realized by connecting any two coincident points, as shown in Fig. 2b. Several GB planes are shown: the CTB, the SITB, and several ATGBs with intermediate inclination angles. The GB periods for the CTB and SITB are defined from either crystal lattice; in this case, the periods for the CTB and SITB are $p_{CTB} = a_0/4[11\bar{2}]$ and $p_{SITB} = a_0[111]$, respectively. The relationship between the inclination angle and the GB periods is defined geometrically as

$$\Phi = \tan^{-1}\left(\frac{m}{n}\frac{|p_{SITB}|}{|p_{CTB}|}\right), \tag{1}$$

where m and n are integers defining the number of CTB and SITB period vectors required to link any two coincident points. An alternative expression is that the ATGB period vector decomposes into the period vectors of the two facets, i.e., $p_{ATGB} = m\, p_{SITB} + n\, p_{CTB}$. At this point, atomistic simulations are then used to calculate the SUs that correspond to the GB periods of the STGBs. For the CTB, the structure can either be defined as a repeating D SU with a period $p_{CTB} = a_0/4[11\bar{2}]$ or as a repeating |*D.D*| SU with a period $p_{CTB} = a_0/2[11\bar{2}]$. The latter SU description is chosen because it contains additional information about the translation of SUs with respect to each

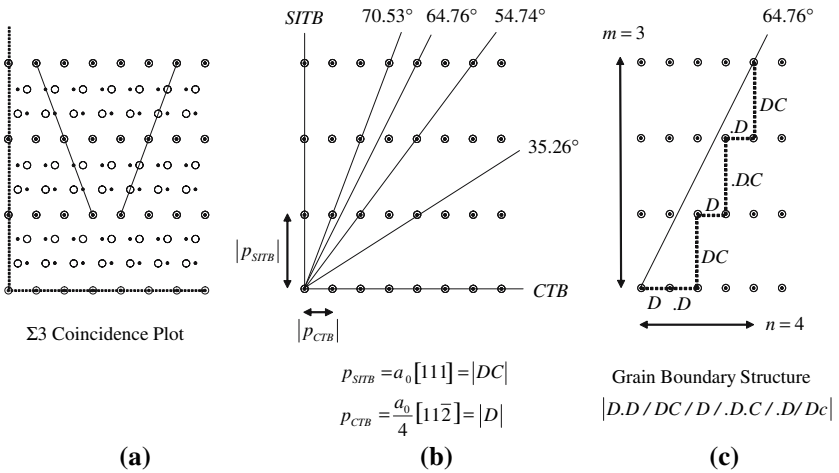

Fig. 2 A model describing the structural units and faceting in Σ3 ATGBs. (a) Coincident plot for the Σ3 system rotated around the $[1\bar{1}0]$ tilt axis. (b) Schematic of the coincident points from (a) along with several GB planes of varying inclination angles. The GB periods of the CTB and SITB correlate to specific atomic SUs. (c) The SU description of the $\Sigma3(554)_1/(11\bar{8})_2\Phi = 64.76°$ ATGB is predicted based solely on the coincident points from (a) and the SUs from the two Σ3 STGBs. Compare to Table 2 and Fig. 1d

other; recall that the dot preceding a SU denotes a relative translation in the direction of the tilt axis by $a_0/4[1\bar{1}0]$. This SU description requires n to be an even integer. Figure 2c shows how the coincident lattice sites from (a), the GB plane from (b), and the STGB SUs are combined to predict the ATGB SU description for the $\Sigma3(554)_1/(11\bar{8})_2\Phi = 64.76°$ ATGB. Until this point, this description only determines the number of SUs on each facet, but there are still a few rules that govern the number and translation of SUs on each facet. The rules for the Σ3 ATGB structures are:

1. For $\Phi \leq 70.53°$, all $|DC|$ SUs on the SITB facet are separated by at least one D SU on the CTB facet. Additionally, for $\Phi \geq 70.53°$, all D SUs on the CTB facet should be separated by at least one $|DC|$ SU on the SITB facet. As observed in (c), this rule minimizes the number of SUs on each facet and maximizes the number of facets.
2. For all SITB facet SUs following a D SU on the CTB, there is a translation involved, i.e., they are $|.D.C|$ SUs. Additionally, for all SITB facet SUs following a $|.D|$ SU on the CTB, there is no translation involved, i.e., they are $|DC|$ SUs. This SU translation is assigned purely by the convention used in this paper to distinguish between SUs with relative translations of $a_0/4[110]$; the $|.D.C|$ and $|DC|$ may be switched in the previous statements and still be correct.

Notice that the ATGB SU description for the $\Sigma3(554)_1/(11\bar{8})_2\Phi = 64.76°$ GB predicts the same SU description as the calculated GB structure shown in Fig. 1d and listed in Table 2. Furthermore, this method for Σ3 ATGBs accurately predicts the GB SU description for all 23 Σ3 ATGBs in this study, even with the 9*R* phase formed for ATGBs with $\Phi \geq 70.53°$ in Cu. Interestingly, especially considering the multiplicity of possible grain boundary structures [44], the lowest energy structures for all Σ3 ATGBs in Cu and Al follow this model for structural units and faceting. This is most likely due to the low energy of the coherent twin boundary. Since this description fits the minimum energy Σ3 ATGB structures calculated in these 0 K simulations, this can be useful in describing the atomic structure of Σ3 ATGBs in terms of SUs or partial dislocations for higher scale computational models that incorporate GB structure. However, it is not apparent whether this description or these rules hold for systems with more complex GB structures at the STGBs. Future work will investigate the structural unit and faceting for other low order CSL ATGB systems [45].

In summary, atomistic simulations are used to examine the structure of 23 Σ3 asymmetric tilt grain boundaries (Table 1) in Cu and Al. The structures obtained (Fig. 1) are characterized in terms of structural units to show that Σ3 asymmetric tilt grain boundaries facet into coherent twin and incoherent twin facets, as in previous studies for Cu [23, 24]. The current simulations provide the following conclusions:

1. The structural units and facets characterized for each of the 23 Σ3 asymmetric tilt grain boundaries (Table 2) are identical in low stacking fault energy Cu and high stacking fault energy Al. The influence of the stacking fault energy in these two FCC metals is negligible with respect to the structural units and facets present in the minimum energy Σ3 grain boundary structure. However, compared to Al, the stacking fault energy in Cu

results in a greater dissociation width of the D structural unit (partial dislocation) on the incoherent twin facet; this leads to the experimentally observed 9R phase in Cu.

2. A method that predicts the calculated structural units and facets in Cu and Al is presented for Σ3 asymmetric tilt grain boundaries (Fig. 2). This method is based on the structural unit model [2], the coincidence plot [42], strip method of quasicrystallography [1, 43] and the atomistic GB structures of the two Σ3 STGBs. The structural unit and faceting description of all 23 calculated grain boundary structures in Cu and Al correlate with this model.

Acknowledgements This material is based upon work supported under a NSF Graduate Research Fellowship. This work was partially supported by the National Center for Supercomputing Applications under DMR060019N and utilized Cobalt. Additional support of the IHPCL at the Georgia Tech College of Computing is acknowledged. D.L.M. is grateful for the support of the Carter N. Paden, Jr. Distinguished Chair in Metals Processing for additional support of this work.

References

1. Sutton AP, Balluffi RW (1995) Interfaces in crystalline materials. Clarendon Press, Oxford
2. Sutton AP, Vitek V (1983) Philos Trans R Soc Lond A 309:37
3. Rittner JD, Seidman DN, Merkle KL (1996) Phys Rev B 53:4241
4. Bishop GH, Chalmers B (1968) Scr Metal 2:133
5. Sutton AP, Vitek V (1983) Philos Trans R Soc Lond A 309:55
6. Rittner JD, Seidman DN (1996) Phys Rev B 54:6999
7. Pawaskar DN, Miller R, Phillips R (2001) Phys Rev B 63:214105
8. Tschopp MA, Tucker GJ, McDowell DL (2007) Acta Mater, doi:10.1016/j.actamat.2007.03.012
9. Suzuki A, Mishin Y (2003) Interface Sci 11:425
10. Suzuki A, Mishin Y (2003) Interface Sci 11:131
11. Janssens K, Olmsted D, Holm E, Foiles S, Plimpton S, Derlet P (2006) Nat Mater 5:124
12. Traut Z, Upmanyu M, Karma A (2006) Science 314:632
13. Sansoz F, Molinari JF (2004) Scr Mater 50:1283
14. Sansoz F, Molinari JF (2005) Acta Mater 53:1931
15. Spearot DE, Jacob KI, McDowell DL (2005) Acta Mater 53:3579
16. Spearot DE, Jacob KI, McDowell DL (2006) Int J Plasticity 23:143
17. Spearot D, Tschopp M, Jacob K, McDowell D (2007) Acta Mater 55:705
18. Hofmann D, Finnis MW (1994) Acta Metall Mater 42:3555
19. Schmidt C, Ernst F, Finnis MW, Vitek V (1995) Phys Rev Lett 75:2160
20. Ernst F, M.W. Finnis, Hofmann D, T.Muschik, Schonberger U, Wolf U, Methfessel M (1992) Phys Rev Lett 69:620
21. Schiøtz J, Di Tolla FD, Jacobsen KW (1998) Nature 391:561
22. Zhang H, Srolovitz DJ (2006) Acta Mater 54:623
23. Wolf U, Ernst F, Muschik T, Finnis MW, Fischmeister HF (1992) Philos Mag A 66:991
24. Ernst F, Finnis MW, Koch A, Schmidt C, Straumal B, Gust W (1996) Zeitschrift fur Metallkunde 87:911
25. Tschopp MA, McDowell DL (2007) Philos Mag, doi: 10.1080/14786430701255895
26. Saylor DM, Morawiec A, Rohrer GS (2003) Acta Mater 51:3663
27. Saylor DM, El Dasher BS, Rollett AD, Rohrer GS (2004) Acta Mater 52:3649
28. Kim C-S, Hu Y, Rohrer GS, Randle V (2005) Scr Mater 52:633
29. Kim C-S, Rollett AD, Rohrer GS (2006) Scr Mater 54:1005
30. Barg AI, Rabkin E, Gust W (1995) Acta Metall Mater 43:4067
31. Hsieh TE, Balluffi RW (1989) Acta Metall 37:2133
32. Straumal BB, Polyakov SA, Bischoff E, Gust W, Mittemeijer EJ (2001) Interface Sci 9:287
33. Lee SB, Sigle W, Ruhle M (2003) Acta Mater 51:4583
34. Straumal BB, Semenov VN, Khruzhcheva AS, Watanabe T (2005) J Mater Sci 40:871
35. Straumal BB, Polyakov SA, Bischoff E, Gust W, Baretzky B (2005) Acta Mater 53:247
36. Straumal BB, Polyakov SA, Mittemeijer EJ (2006) Acta Mater 54:167
37. Minkwitz C, Herzig C, Rabkin E, Gust W (1999) Acta Mater 47:1231
38. Miyamoto H, Ikeuchi K, Mimaki T (2004) Scr Mater 50:1417
39. Mishin Y, Mehl MJ, Papaconstantopoulos DA, Voter AF, Kress JD (2001) Phys Rev B 63:224106
40. Mishin Y, Farkas D, Mehl MJ, Papaconstantopoulos DA (1999) Phys Rev B 59:3393
41. Kelchner CL, Plimpton SJ, Hamilton JC (1998) Phys Rev B 58:11085
42. Kronberg ML, Wilson FH (1949) Am Inst Mining Metall Eng—J Metals 1:501
43. Sutton AP (1988) Acta Metall 36:1291
44. Wang G, Sutton AP, Vitek V (1984) Acta Metall 32:1093
45. Tschopp MA, McDowell DL (2007) Philos Mag, submitted for publication